The Journal of Chemical Physics

RESEARCH ARTICLE | APRIL 28 2025

Correlated vibrational coherence and spectral diffusion analysis of multi-level systems using two-dimensional electronic spectroscopy

Special Collection: David Jonas Festschrift

Sanjib Jana ; Sachin Prasad ; Hoang Long Nguyen ; Duc Viet Le ; Howe-Siang Tan

J. Chem. Phys. 162, 164311 (2025)
https://doi.org/10.1063/5.0268218

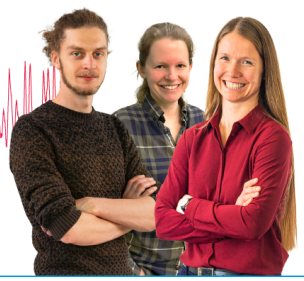

AIP Publishing

The Journal of Chemical Physics ARTICLE pubs.aip.org/aip/jcp

Correlated vibrational coherence and spectral diffusion analysis of multi-level systems using two-dimensional electronic spectroscopy

Cite as: J. Chem. Phys. 162, 164311 (2025); doi: 10.1063/5.0268218
Submitted: 28 February 2025 • Accepted: 7 April 2025 •
Published Online: 28 April 2025

Sanjib Jana, Sachin Prasad, Hoang Long Nguyen, Duc Viet Le,[a] and Howe-Siang Tan[b]

AFFILIATIONS

School of Chemistry, Chemical Engineering and Biotechnology, Nanyang Technological University, 21 Nanyang Link, Singapore 637371

Note: This paper is part of the JCP Special Topic, David Jonas Festschrift.
[a]**Present address:** Institute for Chemical Sciences and Engineering (ISIC), Ecole Polytechnique Fédérale de Lausanne (EPFL), 1015 Lausanne, Switzerland.
[b]**Author to whom correspondence should be addressed:** howesiang@ntu.edu.sg

ABSTRACT

Two-dimensional electronic spectroscopy (2DES) is used to theoretically and experimentally study a minimal three level "V" system (3LVS) with one ground state and two excited states coupled to common displaced harmonic oscillator modes. The third order non-linear optical response functions with frequency fluctuation correlation functions and frequency fluctuation cross correlation functions were derived using the displaced harmonic oscillator model to characterize the diagonal and cross-peaks. The two lowest vibronic transitions of a 6,13-bis(triisopropylsilylethynyl)-pentacene (TIPS-Pn) molecule serve as a model system for the 3LVS considered above. TIPS-Pn's 2DES spectra were measured and analyzed using the center line slope (CLS) method. The CLSs of both the diagonal and cross-peaks consist of an exponential decay and an underdamped mode oscillating at a frequency of 264 cm^{-1}, corresponding to the long axis breathing mode of the pentacene moiety of TIPS-Pn. The CLS oscillations' amplitude and phase of both the diagonal and cross-peaks were measured to have a specific relationship with each other, which is well predicted and simulated by our theory for the 3LVS of TIPS-Pn. We estimate an effective Huang–Rhys factor of ~0.27, which quantifies the coupling of the two vibronic transitions to the long axis breathing mode of the pentacene moiety of TIPS-Pn. We show that such simultaneous CLS analysis recovering the amplitudes and phase relationships between diagonal peaks and cross-peaks measures the correlated vibrational coherences of different states. This can be used to quantify how different excited states or multi-chromophoric states are coupled to common modes in more complex multistate systems.

INTRODUCTION

Two-dimensional electronic spectroscopy (2DES) is a powerful tool and has been used to study the transient dynamics of a variety of complex systems.[1–6] In 2DES, a sequence of three ultrafast pulses interacts with a material system, generating a third-order nonlinear optical signal, which is then measured, analyzed, and presented in a two dimensional spectrum.[7–9] One can view 2DES as an upgrade on the conventional pump–probe or transient absorption spectroscopy technique.[3–5] Excitation frequency resolution is not usually achieved in a conventional broadband pump–probe or transient absorption spectrum. In comparison, on a 2DES spectrum, excitation frequency resolution is achieved. Apart from the "transient absorption" or intensity vs detection axis, a 2DES spectrum has an additional axis corresponding to the excitation frequency.

In a 2DES spectrum of a multi-level system, there will be diagonal and cross-peaks that correlate the excitation frequency to the detection frequency for various processes. The shapes and amplitudes of these peaks vary according to the time delay T_w of the 2DES experiment and contain a wealth of information about the energy transfer dynamics, system–environment interactions, intraband electronic coherences, and vibrational coherences of complex

systems containing multiple states and transitions. The time dependent amplitudes of the diagonal and cross-peaks indicate the population dynamics of the states,[7,8,10,11] whereas the peak shapes encode the interaction of the system with the surrounding bath environment at the molecular level.[9,12] Furthermore, studying the beating patterns of the spectral features allows for information on intra-band electronic coherences and vibrational coherences in complex molecular systems to be extracted.[5,13–15]

The 2DES peak shapes of molecular transitions are strongly influenced by the coupling of electronic states to solvent and vibrational modes.[16–19] The peak shape can be modeled by various methods.[16,18,20–22] Using the well-established Kubo lineshape theory,[23] the 2D spectral peak shape can be modeled by considering the frequency fluctuations of individual transitions. On a 2DES spectrum, the diagonal peak corresponding to a transition to state $|i\rangle$ with transition frequency ω_i is quantified by the frequency fluctuation correlation function (FFCF), $C_{ii}(t) = \langle \delta\omega_i(t)\delta\omega_i(0)\rangle$. The angle bracket, $\langle\cdots\rangle$, represents the equilibrium ensemble average of how a transition with energy gap $\omega_i(t)$ fluctuates or modulates with time.

A microscopic description to model the FFCF is described by coupling transitions to Displaced Harmonic Oscillator (DHO)[24] modes, which effectively emulates the fluctuations in the electronic transitions. These DHO modes can describe the coupling of electronic transitions to vibrational modes, and by extending the coupling to a continuum of modes,[24,25] overdamped solvent modes can be simulated. Typically, the overdamped mode results in an exponential decay of the FFCF over the delay time T_w, whereas the underdamped modes add oscillatory terms to the FFCF.[24,26] The described effects manifest as spectral diffusion dynamics and the oscillatory behavior of the spectral features, respectively.

The spectral diffusion contributions from overdamped oscillator modes are often connected to the librational motion or diffusive dynamics of solvent molecules[27] and are assigned timescales ranging from hundreds of femtoseconds to a few picoseconds. In addition, structural inhomogeneity relates to correlation timescales on the order of hundreds of picoseconds to a few nanoseconds.[28,29] Meanwhile, in the case of an underdamped oscillator, the coherent modulation in the transition energies of system states at frequencies corresponding to the coupled vibrational modes can arise either from intra-chromophore vibrational motions or from external solvent modes.[22] Thus, the DHO theory allows the measured 2D diagonal spectral features to be connected to the microscopic physical processes. Conversely, by measuring the FFCF, insights into the microscopic processes at the molecular level can be obtained. The centerline slope (CLS) analysis[30] is regularly applied in 2DES to measure the spectral diffusion dynamics of molecular systems.[31–34] Furthermore, it can also be used to characterize the vibrational coherences in FFCFs.[22,35]

We can also extend the above analysis, that pertains to diagonal peaks, to cross peaks in 2DES spectra. A cross-peak feature on a 2DES spectrum correlates two distinct transitions with frequencies ω_i and ω_j. We can, therefore, also define a frequency fluctuation cross correlation function (FXCF),[36] $C_{ij}(t) = \langle \delta\omega_i(t)\delta\omega_j(0)\rangle$, which describes the shape of a cross-peak corresponding to excitation at state $|j\rangle$ and detection at state $|i\rangle$. The FXCF is important for multi-level systems such as multi-chromophoric, multi-excitonic systems, or molecular systems with multiple electronic and vibronic transitions. This can be achieved by generalizing the coupling of the two states to a common DHO mode.[37] The FXCFs of the Q_x and Q_y transitions in phthalocyanine (H_2Pc) dissolved in 1-chloronaphthalene were measured recently,[38] which has shown how the different processes contribute to spectral diffusion. It also showed certain degrees of freedom that are coupled in an anticorrelated manner.[38,39] The DHO theory can be extended to model the peak shape of the cross-peaks on 2DES spectra. As in the case of FFCF, an oscillatory feature on the FXCF indicates correlated periodic frequency modulations of two different states coupled to a common underdamped mode. The amplitude of oscillation is determined by the joint coupling strength of the states to the underdamped mode. Although in the previous work, oscillations in the CLS of the cross-peaks were observed, it proved to be too complex to analyze and explain.[38]

In this article, based on the third-order nonlinear optical response theory framework,[24,40,41] we develop a theory using the DHO model to account for the underdamped modulation and spectral diffusion behavior that features on the 2DES spectra of a multi-level system. We then perform a 2DES study on a simple molecular system to demonstrate and validate our theory. We first present the theory applicable to a simple multi-state three level "V" system (3LVS) consisting of one ground state and two excited states, with both the excited state transitions coupled to a common DHO. We use 6,13-bis(triisopropylsilylethynyl) (TIPS)-pentacene (TIPS-Pn) as a model system for our 2DES study. The steady-state absorption spectrum of TIPS-Pn can be described by a two level system (TLS) coupled to a high-frequency vibrational mode, effectively giving rise to two vibronic peaks corresponding to the 0–0 and 0–1 transitions, energetically separated by ~1340 cm^{-1}.[35] This high frequency vibration corresponds to the short-axis C–C stretching vibration of TIPS-Pn having a strong Raman cross-section.[42] Furthermore, the system has a low frequency[35] 264 cm^{-1} mode that couples strongly to the TLS. This mode corresponds to the long axis breathing mode of the pentacene moiety of TIPS-Pn. We show that this system effectively becomes a 3LVS, with equivalent coupling strengths or Huang–Rhys factors based on the DHO model for both the 0–0 and the 0–1 transitions. Using TIPS-Pn as a test system, we performed 2DES and the CLS analysis on the diagonal and off-diagonal cross-peaks to measure and quantify the time dependent peak shape. The CLS analysis revealed spectral diffusion dynamics in both the diagonal and cross-peaks arising from the solvent relaxation dynamics of TIPS-Pn. In addition to spectral diffusion, the CLSs of TIPS-Pn exhibit strong oscillations with a beating frequency of ~264 cm^{-1} on both the diagonal and cross-peaks. The DHO model is able to quantitatively explain the observed behavior in the 2D spectra. The Huang–Rhys factors are then estimated from the diagonal and cross-peaks that quantify the coupling strengths with an underdamped molecular vibrational mode of frequency ~264 cm^{-1}.

THEORY

We first consider a 3LVS, which comprises a common ground state $|g\rangle$ and two excited states $\{|i\rangle, |j\rangle\}$. The 2DES spectrum of such a system can be described by two diagonal peaks at $(\omega_{ig},\omega_{ig})$ and $(\omega_{jg},\omega_{jg})$ and two cross-peaks at $(\omega_{ig},\omega_{jg})$ and $(\omega_{jg},\omega_{ig})$, respectively. To account for all the spectral features that contribute to

the 2DES spectra of such a system, we enumerate all the relevant Double-sided Feynman Diagrams (DSFDs).[2,43] These DSFDs schematically describe the feasible coherence transfer pathways within the system, where the pathways contributing to the signal at the diagonal peak position $(\omega_{ig},\omega_{ig})$ and at the cross-peak position at $(\omega_{jg},\omega_{ig})$ are presented in Figs. 1(a) and 1(b), respectively. By swapping indices i and j, the other two possible signal pathways can be enumerated.

We label the pathways as follows:[20] $R_1^{(ij)}(\tau,T_w,t)\left(R_2^{(ij)}(\tau,T_w,t)\right)$ correspond to non-rephasing (rephasing) stimulated emission (SE) processes, whereas, $R_3^{(ij)}(\tau,T_w,t)\left(R_4^{(ij)}(\tau,T_w,t)\right)$ correspond to the rephasing (non-rephasing) ground state bleach (GSB) processes. The analytical expressions corresponding to the DSFDs, i.e., the response functions, have been evaluated in our previous work[31] by considering the cumulants of the transition frequency fluctuations $\delta\omega$ to second order,[24] resulting in

$$R_1^{(ij)}(\tau,T_w,t)=\mu_{jg}^2\mu_{ig}^2\times\exp\left(-i(\omega_{jg}\tau+\omega_{ig}t)\right)\times\exp\left(-g_{jj}(\tau)-g_{ij}^*(T_w)-g_{ii}^*(t)+g_{ij}(\tau+T_w)+g_{ij}^*(T_w+t)-g_{ij}(\tau+T_w+t)\right), \quad (1)$$

$$R_2^{(ij)}(\tau,T_w,t)=\mu_{jg}^2\mu_{ig}^2\times\exp\left(i(\omega_{jg}\tau-\omega_{ig}t)\right)\times\exp\left(-g_{ij}^*(\tau)+g_{ij}(T_w)-g_{ii}^*(t)-g_{ij}^*(\tau+T_w)-g_{ij}(T_w+t)+g_{ij}^*(\tau+T_w+t)\right), \quad (2)$$

$$R_3^{(ij)}(\tau,T_w,t)=\mu_{jg}^2\mu_{ig}^2\times\exp\left(i(\omega_{jg}\tau-\omega_{ig}t)\right)\times\exp\left(-g_{jj}^*(\tau)+g_{ij}^*(T_w)-g_{ii}(t)-g_{ij}^*(\tau+T_w)-g_{ij}^*(T_w+t)+g_{ij}^*(\tau+T_w+t)\right), \quad (3)$$

$$R_4^{(ij)}(\tau,T_w,t)=\mu_{jg}^2\mu_{ig}^2\times\exp\left(-i(\omega_{jg}\tau+\omega_{ig}t)\right)\times\exp\left(-g_{jj}(\tau)-g_{ij}(T_w)-g_{ii}(t)+g_{ij}(\tau+T_w)+g_{ij}(T_w+t)-g_{ij}(\tau+T_w+t)\right). \quad (4)$$

The lineshape functions $g_{\beta\alpha}(t)$ in the expressions above are defined as

$$g_{\beta\alpha}(t)=\int_0^t d\tau\int_0^\tau d\tau' C_{\beta\alpha}(\tau'), \quad (5)$$

where the states $\{|\alpha\rangle, |\beta\rangle\}$ can represent either $|i\rangle$ or $|j\rangle$. $g_{\beta\alpha}(t)$ represents the auto-correlation lineshape function when $\alpha=\beta$ and the cross correlation lineshape function when $\alpha\neq\beta$. As has been introduced previously, the frequency-gap correlation function $C_{\beta\alpha}(t)=\langle\delta\omega_\beta(t)\delta\omega_\alpha(0)\rangle$ is known as the FFCF when $\alpha=\beta$ and the FXCF when $\alpha\neq\beta$. When $i\neq j$, Eqs. (1) and (2) correspond to population transfer SE processes along the cross-peaks, where the transfer effects incorporated are approximate and are described by a set of rules listed out in our previous work.[31]

The lineshape functions $g_{\beta\alpha}(t)$ in Eqs. (1)–(4) can be cast as a sum of the individual vibrational $g_{\beta\alpha,v}(t)$ and overdamped lineshapes $g_{\beta\alpha,b}(t)$, i.e., $g_{\beta\alpha}(t)=g_{\beta\alpha,v}(t)+g_{\beta\alpha,b}(t)$, which follows from the relation corresponding to the frequency-gap correlation function: $C_{\beta\alpha}(t)=C_{\beta\alpha,v}(t)+C_{\beta\alpha,b}(t)$, where $C_{\beta\alpha,v}(t)$ $[C_{\beta\alpha,b}(t)]$ describes the underdamped [overdamped] frequency correlation function in Eq. (5).

The DHO model[24,26] is well used in providing the microscopic description to model a TLS coupled to an oscillating mode. For an undamped mode ω_v, the auto-correlation function corresponding to state $|i\rangle$, i.e., $C_{ii,v}(t)$, can be expressed as[13]

$$C_{ii,v}(t)=\omega_v^2 S_{ii,v}(\Theta_v(T)\cos(\omega_v t)-i\sin(\omega_v t)), \quad (6)$$

where $\Theta_v(T)=\coth\left(\frac{\hbar\omega_v}{2k_BT}\right)$. $S_{ii,v}=\frac{1}{2}d_i^2=\frac{\lambda_{ii,v}}{\omega_v}$ is the Huang–Rhys factor[24,35] in which $\lambda_{ii,v}$ quantifies the coupling strength to the vibrational mode ω_v and the parameter d_i is the dimensionless shift of the minima of the excited state potential energy surface relative to the ground state along the mode Q_v (Fig. 2).

We can adapt the DHO theory to model the associated FXCF $(\alpha=j,\beta=i)$ for the 3LVS (described in Fig. 2). The detailed derivation is provided in the supplementary material. The resulting FXCF takes a similar form as Eq. (6),

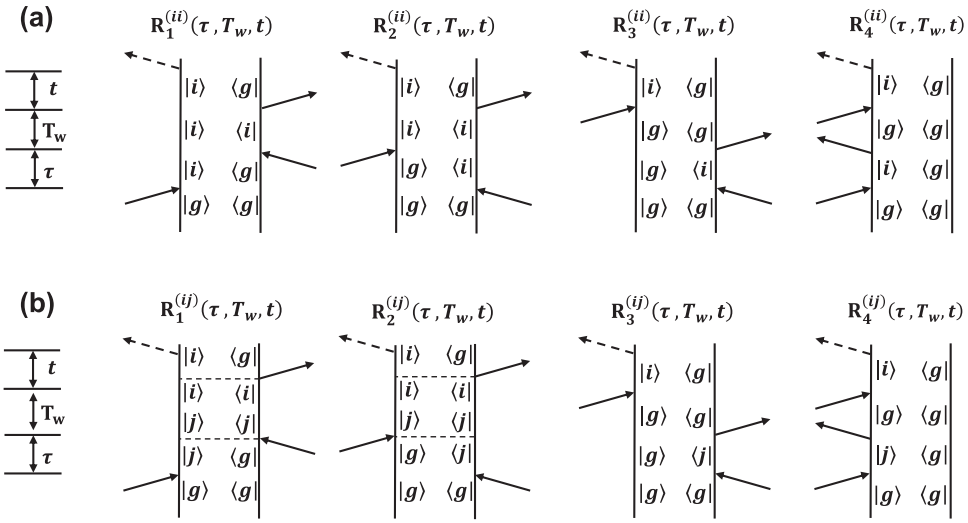

FIG. 1. DSFDs representing the coherence transfer pathways contributing to the (a) diagonal peak at $(\omega_{ig}, \omega_{ig})$ and (b) cross-peak at $(\omega_{jg}, \omega_{ig})$ in the 2DES spectrum. Time runs upwards in the diagrams.

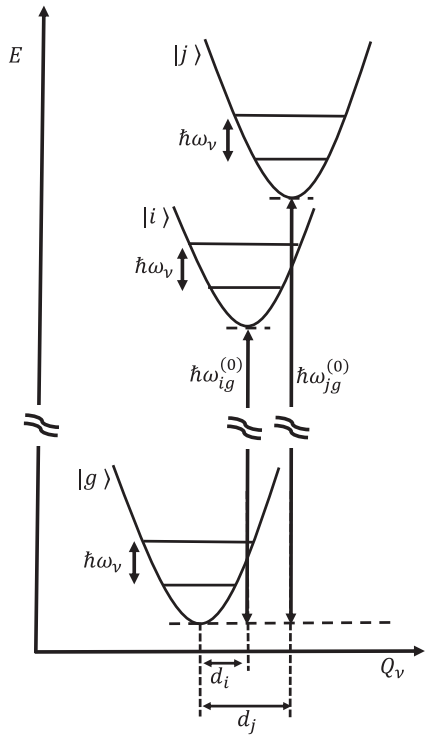

FIG. 2. Schematic representation of the displaced harmonic oscillator representing the coupling of the 3LVS to the harmonic mode Q_v with frequency ω_v.

$C_{ij,v}(t) = \omega_v^2 S_{ij,v}(\Theta_v(T)\cos(\omega_v t) - i\sin(\omega_v t))$, with a cross-Huang–Rhys factor, $S_{ij,v} = \frac{1}{2}d_i d_j$, where d_i and d_j represent the dimensionless displacements of the minima of the two excited state potential energy relative to the ground state, along the vibrational mode Q_v (as shown in Fig. 2). Here, the cross-Huang–Rhys factor determines the undamped oscillation amplitude of $C_{ij,v}(t)$. We can phenomenologically introduce damping into $C_{\beta\alpha,v}(t)$ of a 3LVS with both excited states coupled to the same DHO modes,

$$C_{\beta\alpha,v}(t) = \omega_v^2 S_{\beta\alpha,v}(\Theta_v(T)\cos(\omega_v t) - i\sin(\omega_v t))\exp(-\gamma_{\beta\alpha,v}t), \tag{7}$$

where $\gamma_{\beta\alpha,v}^{-1}$ is a damping constant accounting for the correlation timescale of the underdamped mode.

Similarly, we can model the overdamped contribution of the correlation function, $C_{\beta\alpha,b}(t)$ for the 3LVS. We consider that the system is coupled to a continuum of harmonic bath modes described by the Drude spectral density,[24,25] $\tilde{C}''_{\beta\alpha,b}(\omega) = 2\lambda_{\beta\alpha}\frac{\gamma_{\beta\alpha}\omega}{\omega^2+\gamma_{\beta\alpha}^2}$, where $\gamma_{\beta\alpha}^{-1}$ is the correlation timescale corresponding to a particular overdamped mode, and $\lambda_{\beta\alpha}$ is the reorganization energy quantifying the strength of coupling of the states to the mode. $\lambda_{\beta\alpha}$ is obtained from the relationship $\Lambda_{\beta\alpha} = \frac{2k_BT}{\hbar}\lambda_{\beta\alpha}$. The corresponding frequency-gap correlation function $C_{\beta\alpha,b}(t)$ can be described under the high-temperature limit as

$$C_{\beta\alpha,b}(t) = \Lambda_{\beta\alpha}\exp(-\gamma_{\beta\alpha}t), \tag{8}$$

where we ignore the imaginary component of $C_{\beta\alpha,b}(t)$, assuming the spectral linewidths to be much larger than observed Stokes shifts.[24] We note that, in principle, the theoretical basis of the overdamped and underdamped correlations is similar. The overdamped contribution can be viewed as coupling to a continuous distribution of DHOs.[24] As the later discussions will show, the underdamped part of the correlation functions describes the vibronic coherent modulations, while the overdamped part describes the spectral diffusion process.

With the above models of underdamped and overdamped correlation functions in Eqs. (7) and (8), we carry out the double time integral as described in Eq. (5) to obtain the corresponding lineshape functions. The calculated lineshape functions take the following forms:

$$g_{\beta\alpha,v}(t) = -i\omega_v S_{\beta\alpha,v}t + S_{\beta\alpha,v}\left[\Theta_v\left(1-\cos(\omega_v t)\exp(-\gamma_{\beta\alpha,v}t)\right) + i\sin(\omega_v t)\exp(-\gamma_{\beta\alpha,v}t)\right], \tag{9}$$

$$g_{\beta\alpha,b}(t) = \Gamma_{\beta\alpha}t + \sum_k\left(\frac{\Lambda_{\beta\alpha,k}}{\gamma_{\beta\alpha,k}^2}\right)\left[e^{-\gamma_{\beta\alpha,k}t} + \gamma_{\beta\alpha,k}t - 1\right]. \tag{10}$$

Here, the index "k" represents the contribution of the kth overdamped bath mode in the lineshape function with distinct rate constant $\gamma_{\beta\alpha,k}$. The above derivation is adapted to describe the correlation dynamics of TIPS-Pn, where the system is coupled to an underdamped vibrational mode and overdamped solvent modes. The lineshape function $g_{\beta\alpha,b}(t)$ encodes the overdamped spectral diffusion dynamics and causes the exponential decay of frequency correlation functions, FFCF and FXCF. A homogeneous dephasing rate, $\Gamma_{\beta\alpha}$, is added to $g_{\beta\alpha,b}(t)$. As shown in our previous work,[38] this parameter contributes to the lineshape only for the diagonal peak and cancels out for the cross-peaks in the response function described in Eqs. (1)–(4). Next, the lineshape function $g_{\beta\alpha,v}(t)$ accounts for the underdamped oscillation in the FFCF and FXCF. The complete lineshape function, $g_{\beta\alpha}(t) = g_{\beta\alpha,v}(t) + g_{\beta\alpha,b}(t)$, serves as an input for Eqs. (1)–(4).

Following the above discussion on the general 3LVS, we now discuss the case of our model system, TIPS-Pn. As mentioned earlier, the steady-state absorption of TIPS-Pn in the visible spectrum consists of two vibronic peaks corresponding to the 0–0 and the 0–1 transitions separated by 1340 cm^{-1}. Furthermore, the transitions are coupled to another 264 cm^{-1} vibrational mode. This system of two electronic states, ground and excited states coupled to two vibrational modes, can be shown as an effective quasi-three-level system akin to the 3LVS described above. We start with considering an electronic TLS with a ground state $|g\rangle$ and an excited state $|e\rangle$ coupled to two vibrational modes with frequencies ω_1 and ω_2 ($\omega_1 < \omega_2$). The 0–0 transition energy is $\omega_{eg}^{(0)}$. The vibrational modes are described by the respective number states $|n_1\rangle$ and $|n_2\rangle$. To describe the coupling of a TLS to two modes, we make use of a 2D-DHO model with dimensionless displacements of d_1 and d_2, as shown in Fig. 3(a). The Hamiltonian of the ground and excited potential surfaces can be described as

$$\hat{H}_g = \frac{\hbar\omega_1}{2}\left(\hat{P}_1^2 + \hat{Q}_1^2\right) + \frac{\hbar\omega_2}{2}\left(\hat{P}_2^2 + \hat{Q}_2^2\right), \tag{11}$$

$$\hat{H}_e = \hbar\omega_{eg}^{(0)} + \frac{\hbar\omega_1}{2}\left(\hat{P}_1^2 + \left(\hat{Q}_1 - d_1\right)^2\right) + \frac{\hbar\omega_2}{2}\left(\hat{P}_2^2 + \left(\hat{Q}_2 - d_2\right)^2\right), \tag{12}$$

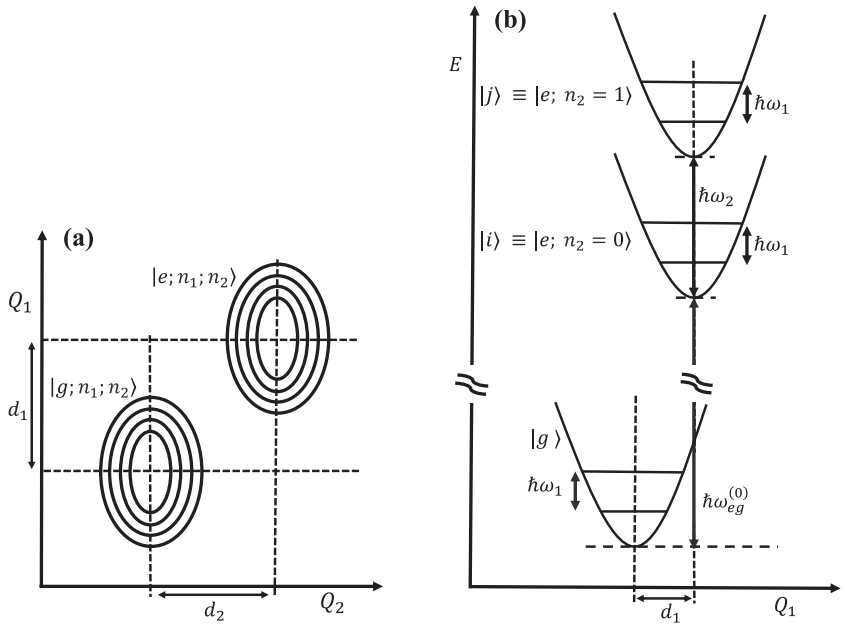

FIG. 3. Schematic diagrams describing (a) a TLS coupled to two vibrational modes having frequencies ω_1 and ω_2 ($\omega_1 < \omega_2$), respectively. (b) The equivalent 3LVS described by projecting the 2D potential map in (a) onto the mode with frequency ω_1.

where $\widehat{P}_k$ and $\widehat{Q}_k$ represent the dimensionless momentum and coordinate operators of the mode with frequency ω_k, respectively. We define the bosonic annihilation operator, $\widehat{a}_k$ and creation operator, $\widehat{a}_k^\dagger$, obeying commutator relation $\left[\widehat{a}_k, \widehat{a}_l^\dagger\right] = \delta_{kl}$. This allows us to recast the momentum $\widehat{P}_k$ and coordinate $\widehat{Q}_k$ operators in terms of the bosonic operators as $\widehat{P}_k = -\frac{i}{\sqrt{2}}\left(\widehat{a}_k - \widehat{a}_k^\dagger\right)$ and $\widehat{Q}_k = \frac{1}{\sqrt{2}}\left(\widehat{a}_k + \widehat{a}_k^\dagger\right)$, respectively. Next, we calculate the expectation value of the excited state energy for a given n_2 as

$$\begin{aligned}\widehat{H}_{e,n_2} &= \langle n_2|\widehat{H}|n_2\rangle = \hbar\omega_{eg}^{(0)} + \frac{\hbar\omega_1}{2}\left(\widehat{P}_1^2 + \left(\widehat{Q}_1 - d_1\right)^2\right) \\ &+ \frac{\hbar\omega_2}{2}\left\langle n_2\middle|\left(\widehat{P}_2{}^2 + \left(\widehat{Q}_2 - d_2\right)^2\right)\middle|n_2\right\rangle = \hbar\omega_{eg}^{(0)} \\ &+ \frac{\hbar\omega_1}{2}\left(\widehat{P}_1{}^2 + \left(\widehat{Q}_1 - d_1\right)^2\right) + \frac{\hbar\omega_2 d_2^2}{2} \\ &+ \frac{\hbar\omega_2}{2}\left\langle n_2\middle|\left(2\widehat{a}_2^\dagger\widehat{a}_2 + 1\right)\middle|n_2\right\rangle = \hbar\omega_{eg}^{(0)} \\ &+ \frac{\hbar\omega_1}{2}\left(\widehat{P}_1^2 + \left(\widehat{Q}_1 - d_1\right)^2\right) + \hbar\omega S_2 + \hbar\omega_2\left(n_2 + \frac{1}{2}\right). \quad (13)\end{aligned}$$

From Eq. (13), we can calculate the energies corresponding to $n_2 = 0$ and $n_2 = 1$, which are given by

$$\langle\widehat{H}\rangle_{e,n_2=0} = \hbar\omega_{eg}^{(0)} + \frac{\hbar\omega_1}{2}\left(\widehat{P}_1^2 + \left(\widehat{Q}_1 - d_1\right)^2\right) + \frac{1}{2}\hbar\omega_2 + \hbar\omega_2 S_2\,, \quad (14)$$

$$\langle\widehat{H}\rangle_{e,n_2=1} = \hbar\omega_{eg}^{(0)} + \frac{\hbar\omega_1}{2}\left(\widehat{P}_1^2 + \left(\widehat{Q}_1 - d_1\right)^2\right) + \frac{3}{2}\hbar\omega_2 + \hbar\omega_2 S_2\,. \quad (15)$$

Equations (14) and (15) are the energies corresponding to 1D excited surfaces in Fig. 3(b) and the Huang–Rhys factor, $S_2 = \frac{d_2^2}{2}$.

This derivation transforms a TLS coupled to two vibrational modes into a quasi-3LVS coupled to one vibrational mode, with the two vibronic peaks originating from the 0–0 and the 0–1 Franck–Condon transitions along the 1340 cm^{-1} ($= \omega_2$) mode as in TIPS-Pn. These vibronic peaks are the "excited" states. The low frequency mode, having a frequency of 264 cm^{-1} ($= \omega_1$), is the "common" mode that both the "excited" states are coupled. Hence, we may treat TIPS-Pn as a special case of the general 3LVS, with $|i\rangle \equiv |e;\ n_2 = 0\rangle$ and $|j\rangle \equiv |e;\ n_2 = 1\rangle$ (Fig. 3). This allows us to use Eqs. (1)–(10) to describe the 2DES spectra. We further note that the shifts in the excited state potential minima of the two excited states are the same, i.e., $d_i = d_j = d_1$, as indicated in Fig. 3(b). This will turn out to make TIPS-Pn a useful model to verify our theoretical considerations made above for the 3LVS. Figure 3(b) shows the schematic diagrams of energy level along normal mode q_v ($= q_1$) and corresponding displacements for the 0–0 and the 0–1 vibronic states of TIPS-Pn. From the above calculation and Fig. 3(b), it is evident that both d_i and d_j have the same sign and numerical value of d_1. 2DES spectra calculated using Eqs. (1)–(4) can be utilized to extract the FFCF, $C_{ii}(t) = \langle\delta\omega_i(t)\delta\omega_i(0)\rangle$, for the diagonal peak and the FXCF, $C_{ij}(t) = \langle\delta\omega_i(t)\delta\omega_j(0)\rangle$, for the cross-peak of TIPS-Pn.[38] We can also account for the periodic oscillatory features in the FFCF and FXCF in addition to the background exponential decay dynamics.

EXPERIMENTAL METHODS

Laser pulses (40 fs time duration, 1 kHz repetition rate, a central wavelength of 790 nm) from a Ti:sapphire regenerative amplifier (Legend Elite, Coherent) were focused into a pressurized argon tube with a pressure of 2.6 bar to generate a white light supercontinuum. This supercontinuum was then passed through a 750 nm short pass filter. The white light supercontinuum then passed through a fused silica wedged window and split into the pump and probe beams. The transmitted pump beam was passed through a prism compressor followed by a pulse shaper (Dazzler, Fastlite). The output

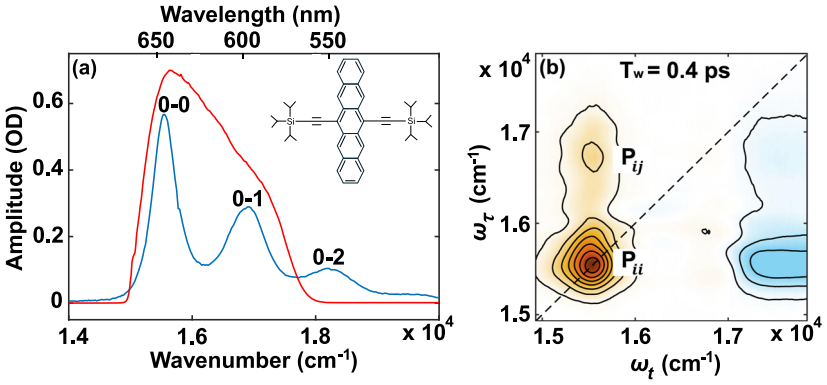

FIG. 4. (a) The steady-state absorption spectrum of TIPS-Pn dissolved in toluene (blue) in the visible region. The red curve is the spectrum of the excitation pump for the 2DES experiment. The inset shows the molecular structure of TIPS-Pn. (b) A representative 2DES spectrum of TIPS-Pn for delay time T_w = 0.4 ps. Two prominent peaks, P_{ii} (diagonal peak) and P_{ij} (cross-peak), are indicated.

beam contains compressed pulses with phase locked double-pulse train for the 2DES experiment. The pulse shaper controls the inter pulse delay τ of this shaped double pulse train. The absorptive 2DES experiment is carried out using a 1 × 2 phase cycling scheme with a pump–probe beam geometry.[44] The inter pulse delay τ was scanned from 0 to 125 fs with 5 fs steps. The output pump pulse had a spectral width of ~3000 cm^{-1} [see Fig. 4(a)] and a pulse duration of 14 fs. The probe beam, reflected from the front surface of the fused silica wedge, was compressed by a pair of chirped mirrors. The probe pulse was delayed by a computer-controlled delay stage (Physik Instrumente). The polarization of the probe beam was set to the magic angle (54.7°) relative to the pump beam by a half wave plate. The pump and probe beams were focused onto the sample cuvette by an off-axis parabolic mirror. The transmitted probe beam was collimated by collection optics and then focused onto the entrance of the spectrometer. The spectrum was detected by a CCD camera (PIXIS) after being dispersed by a grating of 150 grooves/mm. The transient absorption spectra $\Delta A(\tau, T_w, \omega_t)$ were recorded for a series of pump-pulse delays τ. The 2DES spectra for a given T_w, $S^{2D}(\omega_\tau, T_w, \omega_t)$, was then obtained after a Fourier transform along the pump-pulse delay (τ-axis) and further signal processing.[44] In this experiment, T_w was scanned from −100 fs to 2 ps with 10 fs step sizes.

6,13-Bis(triisopropylsilylethynyl) pentacene (TIPS-Pn) was purchased from Sigma Aldrich (≥99%) and used as is without any further purification for the steady-state absorption as well as the 2DES experiment. TIPS-Pn was dissolved in toluene to form a solution with a maximum optical density (OD) of ~0.57 OD at its strongest peak, corresponding to the 0–0 transition in a 1 mm quartz cuvette. The absorption spectrum is shown in Fig. 4(a). The same solution was used to carry out the 2DES measurements.

RESULTS

Figure 4(a) shows the steady-state absorption spectra of TIPS-Pn dissolved in toluene in the visible spectral region. The lowest energy absorption peak at 15 552 cm^{-1} is the 0–0 vibronic peak of TIPS-Pn. There are several other vibronic peaks at higher energy: 0–1 at 16 890 cm^{-1} and 0–2 at 18 250 cm^{-1} followed by a low intensity tail at energies greater than 19 000 cm^{-1}. The best fit of the peaks with Gaussian lineshape functions yields a full width at half maxima (FWHM) of ~460 ± 60 and 820 ± 60 cm^{-1} for the two lowest energy 0–0 and 0–1 vibronic peaks, respectively. The broadband excitation pump in our 2DES experiment has a bandwidth of ~3000 cm^{-1} and covers both the 0–0 and the 0–1 vibronic peaks of TIPS-Pn. The red curve in Fig. 4(a) shows the spectrum of the excitation pump pulses used in the 2DES study.

Figure 5 shows the representative plots of the absorptive 2DES spectra of TIPS-Pn dissolved in toluene for different delay times T_w. The vertical axis of each 2D plot shows the pump frequency, whereas the horizontal axis shows the probe frequency. The dashed line (black) in each plot is the diagonal line where the pump frequency (ω_τ) equals the probe frequency (ω_t). A negative signal on the 2D spectrum comprises GSB and SE processes, whereas a positive signal represents excited state absorption (ESA) processes. Any point (ω_t, ω_τ) on each 2DES plot shows the population at the probe frequency ω_t after the excitation at the pump frequency ω_τ. The delay time dependent changes in the population at each point can be tracked to reveal the transient excited state dynamics of TIPS-Pn.

Figure 5(a) shows the 2DES signal of TIPS-Pn at the delay time T_w = 0.1 ps. A strong diagonal peak P_{ii} centered at (15 552, 15 552) cm^{-1} appears, which is the combination of the GSB and SE signal from the 0–0 vibronic peak. A weak but noticeable diagonal peak P_{jj} centered at (16 890, 16 890) cm^{-1}, represents the 0–1 vibronic peak. Furthermore, a prominent cross-peak P_{ij} appearing on the upper diagonal centered at (16 890, 15 552) cm^{-1} is due to the combination of "downhill" population transfer from the 0–1 vibronic state to the lower 0–0 vibronic state, which occurs on a timescale within the pulse duration, and the sharing of common ground state by the 0–0 and 0–1 vibronic states. A very weak lower cross-peak P_{ji} appears for the probe frequency range ω_t = 16 500–17 000 cm^{-1} with the pump frequency ω_τ = 15 552 cm^{-1}. A strong ESA signal appears in the spectral region ω_t > 17 000 cm^{-1}, which interferes with the spectral region ω_t ~ 16 890 cm^{-1}. The 2DES spectrum at a longer delay time, T_w = 0.4 ps, is shown in Fig. 5(b). The lower cross-peak becomes prominent (but is still too weak to be observed clearly) as the intensity of the strong diagonal peak P_{ii} decays. The upper cross-peak becomes very prominent at delay time T_w = 0.4 ps. The shape of the diagonal peak P_{ii} changes from being diagonally elongated at T_w = 0.1 ps to approaching circularity at T_w = 0.4 ps, indicating

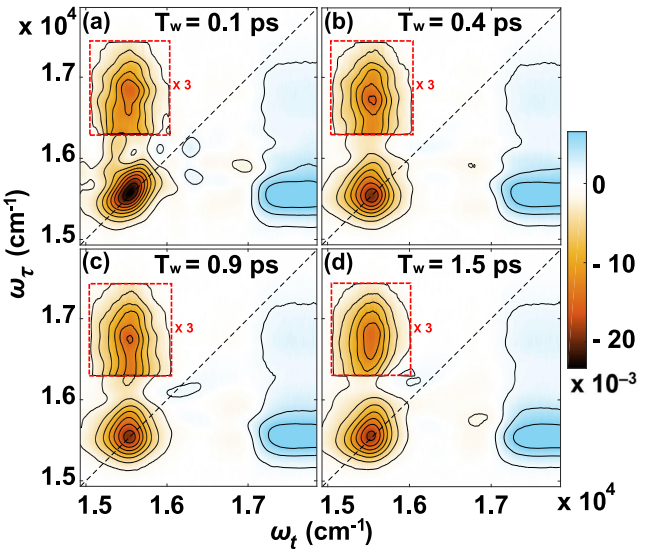

FIG. 5. 2DES spectra for delay times T_w = (a) 0.1 ps, (b) 0.4 ps, (c) 0.9 ps, and (d) 1.5 ps, with a diagonal peak P_{ii} appearing from the 0–0 vibronic peak and an off-diagonal cross-peak P_{ij} appearing due to the combination of "downhill" population transfer from the 0–1 to 0–0 vibronic state and the sharing of common ground state by the 0–0 and 0–1 vibronic states. The pump and the probe frequencies are plotted along the *y*- and *x*-axes, respectively. The black dashed line shows the diagonal where the pump frequency equals the probe frequency. The contours are spaced at 10% of the highest intensity of the color bar. The 2DES spectrum region of the P_{ij} cross-peak is enhanced by a factor of 3 (red box) for more clarity. The unenhanced 2DES spectra are presented in the supplementary material (Fig. S2).

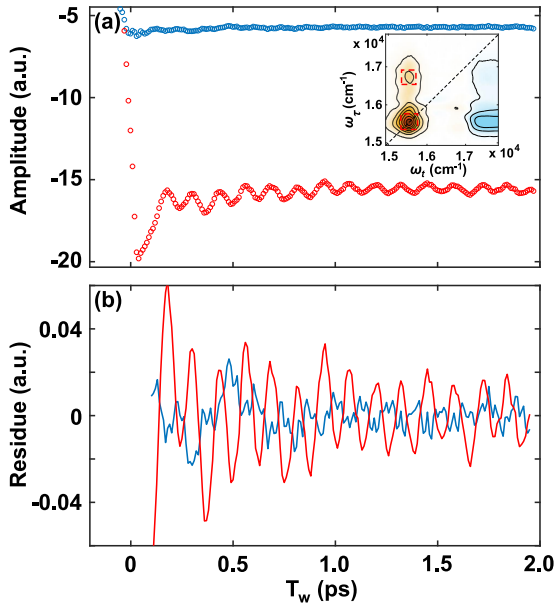

FIG. 6. (a) The time dependent dynamics of the integrated intensities of the 2DES spectra (red-colored boxes on the inset) at the diagonal P_{ii} (red) and the cross-peak P_{ij} (blue). (b) The intensity-normalized residual time-dependent oscillation amplitude of the integrated intensities of (a).

spectral diffusion. Similar dynamics follow at the longer delay times shown in Figs. 5(c) and 5(d). Owing to the low intensity of the upper diagonal and the lower cross-peak, we henceforth will only focus on the lower diagonal peak P_{ii} and the upper cross-peak P_{ij} for our further analysis. A representative figure with enhanced amplitude for the upper diagonal P_{jj} and the lower cross-peak P_{ji} is presented in Fig. S5 of the supplementary material.

Figure 6(a) shows the time dependent intensity dynamics of the diagonal and cross-peaks, extracted by integrating the intensity of the spectral region (red-colored boxes on the 2DES of the inset) of the 2DES signal. A strong oscillation with a period of ~126 ± 10 fs is observed with a slowly decaying background for the diagonal peak (red). The integrated intensity of the cross-peak rises at early delay time (within the pulse width of the laser) and shows little decay within 1 ps, followed by negligible change up to the experimental delay time limit of T_w = 2 ps. An exponential function is employed to subtract the decaying amplitude and extract the residual oscillatory feature. The corresponding oscillation frequency of ~264 ± 13 cm^{-1} is obtained by the Fourier transform of the residue. A clear oscillation with a similar frequency is also observed for the cross-peak. The residual oscillatory modulation is normalized by the background exponential decay amplitude to quantify the intensity-normalized oscillation amplitude for both the peaks, as shown in Fig. 6(b). This shows that the cross-peak has a relatively lower oscillation amplitude compared to the diagonal. Furthermore, as shown in the supplementary material (Fig. S3), different points on the same peak have different phase relations for both the diagonal and cross-peaks. This is a noteworthy observation compared to the CLS of the diagonal and cross-peaks, as shown in the following sections [Fig. 7(b)], which appear to oscillate in phase.

Next, the diagonal peak P_{ii} and the cross-peak P_{ij} of TIPS-Pn are analyzed to study the time dependent changes in the peak shape to provide the details of the frequency fluctuation correlation functions, FFCF and FXCF, respectively. The CLS method is employed to extract the FFCF and FXCF from the 2DES data of TIPS-Pn. The following procedure is used to extract the CLS. We take several slices of the 2D spectrum at a given delay time T_w along the probe axis around the 2DES peak for a series of pump frequencies. We precisely identify the probe frequency corresponding to the maximum absolute intensity from each of the slices, which is the center point. A linear curve is fitted to the center points of all the slices to get a slope. The inverse of this slope is the CLS for the given delay time T_w. This procedure is repeated for all the delay times to extract the time dependent CLS (T_w) function of TIPS-Pn. Figure 7(a) shows the position of the center points (red and blue curves on the diagonal and cross-peaks, respectively) for the delay time T_w = 1.5 ps.

Figure 7(b) shows the delay time dependent CLS (T_w) for the diagonal peak P_{ii} (red) and the cross-peak P_{ij} (blue). Both the CLSs show a prominent oscillation with a period of ~126 ± 10 fs. The $CLS_{ii}(T_w)$ for the diagonal peak P_{ii} starts with a value of >0.3 and shows an exponential decay together with an oscillatory pattern that damps with delay time T_w. The significant oscillation amplitude is observed even at the limit of our experimental delay time of 2 ps, which indicates that the oscillation persists beyond 2 ps. The $CLS_{ij}(T_w)$ for the cross-peak P_{ij} starts with a value near zero

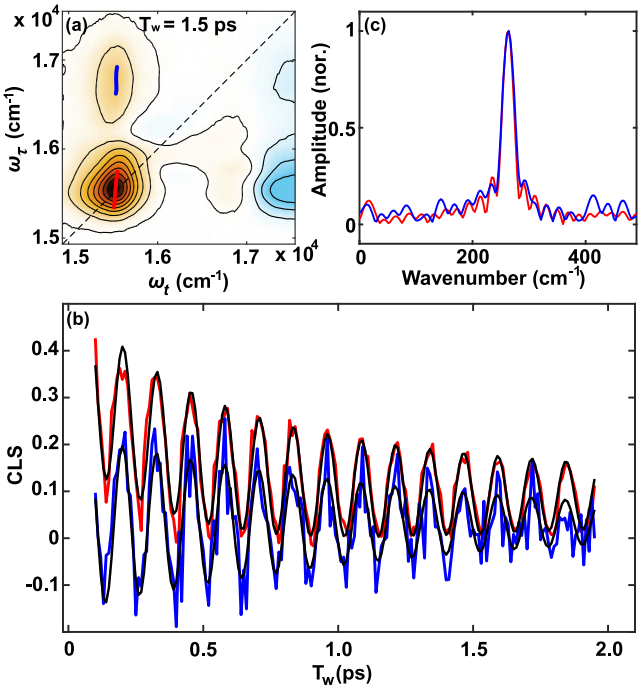

FIG. 7. (a) The center points (red and blue curves for the diagonal and cross-peak, respectively) on the 2DES spectrum at delay time T_w = 1.5 ps. (b) The delay time dependent CLS (T_w) for the diagonal peak (red) and the cross-peak (blue). The black curves are the fit of the corresponding CLSs with an appropriate oscillatory-exponential function. (c) The oscillation frequencies of the corresponding peaks obtained by Fourier transforming the residue of the CLS after subtracting the exponential background. The red (blue) curve is for the diagonal peak (cross-peak).

and shows a damped oscillation. The CLSs of both the diagonal and cross-peaks in Fig. 7(b) appear to oscillate in phase for the entire experimental delay time of 2 ps and have comparable amplitudes. The oscillation frequency is obtained by subtracting the CLS with an appropriate exponential decay function, and the residual oscillation is Fourier transformed. Figure 7(c) shows the normalized plot of the extracted frequencies, which peaks at ~264 cm^{-1} for both the diagonal (red) and the cross-peaks (blue). We employ an oscillatory function with an exponential decay function of the form $CLS(T_w) = a_0 + \Sigma_k a_k e^{-\mu_k T_W} + \Sigma_m b_m e^{-\gamma_m T_W} \cos[\omega_m T_W + K_m \pi]$ to fit the CLS of both peaks. The black curve in Fig. 7(b) shows the resultant best fit. The value of the parameters for the fit is tabulated in Table I. The frequency of the oscillation in the fit is set to 264 cm^{-1}. Table I shows the amplitude (parameter b_1) of the oscillation for both the diagonal and cross-peaks, which are comparable and have the same sign. The phase (parameter K_1) of the oscillation is similar within the error limit at ~0.8π for both peaks. This indicates that both the oscillations for the diagonal and cross-peaks are in phase during the window of our experimental delay time [Fig. 7(b)].

SIMULATION

We simulated the 2DES spectra of TIPS-Pn utilizing the response functions [Eqs. (1)–(4)] outlined in the "Theory section" and extracted the CLS of the diagonal peak P_{ii} and the cross-peak P_{ij} from the spectra. The input parameters for the lineshape functions in the response functions are generated from the experimental fit of the CLS as tabulated in Table I, as well as the experimental absorption spectrum of TIPS-Pn dissolved in toluene [Fig. 4(a)]. In the simulations, we consider the diagonal peak P_{ii} of TIPS-Pn centered at (15 552, 15 552) cm^{-1} and the cross-peak P_{ij} centered at (16 890, 15 552) cm^{-1}. The temperature for the simulation is set at T = 300 K. In the simulation, the delay time T_w is taken from 100 fs to 2 ps with 1 fs time steps.

To simulate the diagonal peak, P_{ii}, we need to generate the lineshape functions $g_{ii}(t)$ in the response functions with its components, $g_{ii,v}(t)$ and $g_{ii,b}(t)$ [Eqs. (9) and (10)]. The parameters needed in these functions are the square of the fluctuation amplitude, $\Lambda_{ii,k}$, the homogeneous rate constant, Γ_{ii}, and the Huang–Rhys factor, S_{ii}. We start by introducing a scaling parameter Λ_{ii}, which is used to obtain the parameter for the amplitude $\Lambda_{ii,k}$ in the lineshape function as $\Lambda_{ii,k} = a_{ii,k}\Lambda_{ii}$. The parameters $a_{ii,k}$ are obtained from the fit (parameters a_k) of the background exponential decay of $CLS_{ii}(T_w)$ in Table I. The scaling parameter Λ_{ii} measures the square of the fluctuation amplitude of the transition and can be estimated by fitting the spectral linewidth of the absorption spectra of the transition. As indicated in Eq. (7), the Huang–Rhys factor determines the oscillation amplitude. We assume the damping constant $\gamma_{ii,v}$ = 0.54 ps^{-1} [in Eq. (7)], which lies within the error range of the experimentally measured damping constant γ_1 of the oscillatory portion of $CLS_{ii}(T_w)$ (we will discuss the choice of $\gamma_{ii,v}$ below). By iteratively fitting the experimental $CLS_{ii}(T_w)$ and the linear spectrum of the 0–0 peak, we obtained the parameters Λ_{ii}, Γ_{ii}, and S_{ii}, which are presented in Table II. A detailed description of the simulation routine is provided in Sec. 4 of the supplementary material. The resultant simulated (black curve) $CLS_{ii}(T_w)$ for the diagonal peak P_{ii} is shown in Fig. 8(b), which matches well with the experimental (red curve) $CLS_{ii}(T_w)$. The simulated absorption spectra for the 0–0 peak overlaid with the experimental absorption spectra are presented in the supplementary material (Fig. S4). The estimated homogeneous

TABLE I. List of values of the parameters for the best fit of the oscillatory and exponential decay function of the CLS in Fig. 7(b). The frequency of the oscillation is set to the experimentally observed mean value, ω_1 = 264 cm^{-1}.

Peak	a_0	a_1	μ_1 (ps^{-1})	b_1	γ_1 (ps^{-1})	K_1
P_{ii}	0.088 ± 0.008	0.278 ± 0.027	2.512 ± 0.425	0.169 ± 0.015	0.449 ± 0.096	0.784 ± 0.015
P_{ij}	0.033 ± 0.007	⋯	⋯	0.189 ± 0.031	0.728 ± 0.203	0.820 ± 0.029

TABLE II. Parameters for the simulation of the CLS for the diagonal and cross-peaks of TIPS-Pn dissolved in toluene. The oscillation frequency for the simulation is ω_v = 264 cm^{-1}, taken from the experimentally obtained value. The temperature for the simulation is assumed to be 300 K.

Peaks	$\Gamma_{\beta\alpha}$ (ps^{-1})	$\Lambda_{\beta\alpha}$ (ps^{-2})	$S_{\beta\alpha,v}$
P_{ii}	25	614	0.27
P_{ij}	⋯	48	0.27
P_{jj}	25	3412	0.27

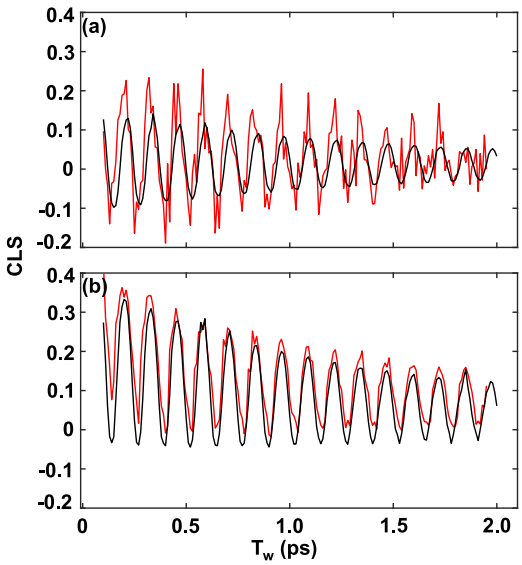

FIG. 8. Simulation of the CLS for the (a) cross-peak and (b) diagonal peak. The black curves show the simulated results, whereas the red curves show the experimental CLS. The parameters obtained from the simulation are tabulated in Table II.

dephasing rate for the P_{ii} peak is Γ_{ii} = 25 ps^{-1}, and the scaling factor is Λ_{ii} = 614 ps^{-2}.

Next, we simulate the $\mathrm{CLS}_{ij}(\mathrm{T_w})$ of the cross-peak P_{ij}. To generate the $\mathrm{CLS}_{ij}(\mathrm{T_w})$ of the cross-peak utilizing Eqs. (1)–(4), the auto-correlated lineshape functions $g_{ii}(t)$ and $g_{jj}(t)$ and the cross-correlated lineshape function $g_{ij}(t)$ are required. We assume that the population transfer from the 0–1 to 0–0 vibronic states is instantaneous and, hence, include both GSB and SE signals in the simulation for all $\mathrm{T_w}$. The auto-correlated lineshape function $g_{ii}(t)$ is available from the procedure outlined in the previous paragraph. However, the other auto-correlated lineshape function $g_{jj}(t)$, which should be obtained by the analysis of the P_{jj} diagonal peak, is not readily available since the peak signal is too weak for any reasonable $\mathrm{CLS}_{jj}(\mathrm{T_w})$ measurement to be carried out. Instead, we will approximate the lineshape function $g_{jj}(t)$ by assuming $C_{jj,b}(t)$ to have similar decay constants as $C_{ii,b}(t)$, and the homogeneous dephasing rate Γ_{jj} to also be similar to Γ_{ii}. We, therefore, obtain the parameters for the lineshape function [Eqs. (9) and (10)] as $\Lambda_{jj,k} = a_{jj,k}\Lambda_{jj}$ with amplitudes $a_{jj,k}$ to be the same as $a_{ii,k}$ used to simulate P_{ii} above. In the simulation, the parameter Λ_{jj} is varied to obtain a best fit to the experimental FWHM of the 0–1 steady-state absorption peak of TIPS-Pn. We fix the parameters for the oscillation to the same values as the P_{ii} peak in accordance with the theory described earlier (Fig. 3), which predicts both the Huang–Rhys factors, $S_{ii,v}$ and $S_{jj,v}$, for both the diagonal peaks to be the same. The simulated absorption spectra for the 0–1 peak overlaid with the experimental absorption spectra are presented in the supplementary material (Fig. S4). For further details and clarification about the simulation, readers are referred to Sec. 4 of the supplementary material. The estimated homogeneous dephasing rate for the P_{jj} peak is Γ_{jj} = 25 ps^{-1}, and the scaling factor is Λ_{jj} = 3412 ps^{-2}, as tabulated in Table II.

Finally, we proceed to obtain the cross-correlated lineshape function $g_{ij}(t)$. The parameters $\Lambda_{ij,k}$, which enter into $g_{ij}(t)$ [see Eq. (10)] can be estimated[38] by its relationship to Λ_{ii} and Λ_{jj} according to the non-oscillatory part of $\mathrm{CLS}_{ij}(\mathrm{T_w})$ at zero time delay ($\mathrm{T_w}$ = 0). In this case, this will be a_0 from Table I and $\overline{C_{ij}}(0) = \mathrm{CLS}_{ij}(0) = \frac{\Lambda_{ij}}{\sqrt{\Lambda_{ii}\Lambda_{jj}}} \sim 0.033$. This results in Λ_{ij} = 48 ps^{-2}, which goes as the input parameter for the $\Lambda_{ij,k}$ in the lineshape function of Eq. (10) (in this case, there is only one $\Lambda_{ij,k}$ for the cross-peak). The homogeneous dephasing rate Γ_{ij} does not appear in the response function as described in Ref. 38. We set S_{ij} to be the same value as S_{ii} or S_{jj}, as the theory predicts that the cross-Huang–Rhys factors and Huang–Rhys factors should have the same numerical value. Furthermore, the damping constant $\gamma_{ij,v}$ [in Eq. (7)] will also be held to be the same as that of $\gamma_{ii,v}$. This constraint arises from the approximation mentioned earlier that the oscillation parameters used in $g_{jj,v}(t)$ are similar to $g_{ii,v}(t)$. This approximation also leads to the equality of all the damping factors $\gamma_{ii,v}$, $\gamma_{jj,v}$, and $\gamma_{ij,v}$. The choice of $\gamma_{ij,v} = \gamma_{ii,v}$ = 0.54 ps^{-1} is made since the value simultaneously lies within the error range of the fitted damping constants γ_1 for the oscillations in both $\mathrm{CLS}_{ii}(\mathrm{T_w})$ and $\mathrm{CLS}_{ij}(\mathrm{T_w})$. The parameters to describe the peak P_{ij} are tabulated in Table II, and the resultant simulated (black curve) $\mathrm{CLS}_{ij}(\mathrm{T_w})$ for the cross-peak is shown in Fig. 8(a), as compared with the experimentally (red curve) obtained CLS.

DISCUSSION

We have presented above, in the "Theory section," a framework to understand the spectral features of a 2D spectrum of a basic multistate system, namely, a 3LVS system with a ground state and two excited states coupled to a common vibrational mode. In this regard, the key results of this work are depicted in Fig. 7(b), where we have the CLS analysis of both the diagonal and cross-peaks. These CLSs can be decomposed into a linear combination of exponential decay and oscillatory terms with the fit parameters listed in Table I. The important observations to note are that for the oscillatory terms' fit parameters, there are definite and meaningful phase and amplitude relationships between the oscillation in the CLS of the diagonal peak P_{ii} and the cross-peaks P_{ij}. In contrast, observing just the 2DES peak intensity oscillation, or the oscillation amplitude of various points on the 2DES spectra, yields complicated amplitude and phase relations (Figs. 6 and S3). The definite phase and intensity of the CLS oscillations at frequency 264 cm^{-1} observed are corroborated in the "Simulation section." As tabulated in Table I, it

can be observed that both the oscillations in the CLS of the diagonal and cross-peaks have comparable amplitudes and similar phases (~0.8π) over the 2 ps delay time window of our experiment. It will be discussed further as to why these observations and results are significant.

In our 3LVS coupled to a common DHO model presented in the "Theory section" [Figs. 2 and 3 and Eqs. (14) and (15)], the resulting FFCF and FXCF include oscillatory terms at the DHO frequency ω_1 as described by Eq. (7). The amplitudes of the FFCF and FXCF depend on the Huang–Rhys factor $S_{ii,v} = \frac{1}{2}d_i^2$ and the cross-Huang–Rhys factor $S_{ij,v} = \frac{1}{2}d_i d_j$, respectively. The parameters d_i and d_j are the shifts of the minima of the potential energy surfaces [Fig. 3(b)] of two excited states that the cross-peak connects [Eq. (S5) of the supplementary material]. Furthermore, in the case of our present model molecule, TIPS-Pn, with a two-level electronic system coupled to two vibrational modes, $\omega_1 = 264\ \mathrm{cm}^{-1}$ and $\omega_2 = 1340\ \mathrm{cm}^{-1}$, this system can be shown to behave like a quasi-3LVS system with one ground state and two vibronic levels (separated by $\omega_2 = 1340\ \mathrm{cm}^{-1}$) having the same shift of potential minima, $d_i = d_j$ [Fig. 3(b) and Eqs. (13)–(15)], for the vibrational manifold with $\omega_1 = 264\ \mathrm{cm}^{-1}$. This entails that the resulting numerical values of both the Huang–Rhys factors and the cross-Huang–Rhys factor of the FFCFs and FXCFs are the same.

The FFCF and FXCF are connected to the measurable CLS analysis of the diagonal and cross-peaks. Simulations were carried out to emulate the time dependent $\mathrm{CLS}_{ii/ij}(\mathrm{T_w})$ for both the diagonal and cross-peaks by utilizing response functions [Eqs. (1)–(4)] described in the "Theory section." By assuming $d_i = d_j$ and, hence, the equality of the Huang–Rhys factors, $S_{ii,v} = S_{jj,v}$, and the cross-Huang–Rhys factor, $S_{ii,v} = S_{ji,v}$, the iterative fits recover an input parameter value of ~0.27 in our simulation. Figure 8 shows that the results obtained from the theoretical model used in the simulations corroborate reasonably well with the experimental CLS. The amplitudes have slight mismatches, especially for cross-peak P_{ij}. This may be due to our simplification of assuming that $C_{jj,b}(t)$ and Γ_{jj} to be similar to $C_{ii,b}(t)$ and Γ_{ii}, as described in the "Simulation section," which is due to the lack of a good measurement of the diagonal peak P_{jj}. For other systems, better fits to the amplitudes can be made if we have measurements of all the relevant diagonal peaks, which is lacking in the system used in this study. On the other hand, the phases present a good match. We note that the inputs for the simulations include only the parameters from the fits in Table I and the lineshape parameters obtained from fitting the linear spectrum. The temperature for the simulations is assumed to be T = 300 K. There are therefore no "floating" parameters used for the simulations to "fix" the phase between the experiment and the simulation. Thus, it is significant that the phases of the oscillations between the simulation and the experiments match up well. This suggests the validity of the general DHO model of the coupling of multi-electronic states (Figs. 2 and 3) to a common vibrational mode. Future simulation analysis will be carried out to understand the temperature dependence of the oscillation amplitude and the phase.

In general, for a 3LVS, the displacements of the potential minima for the two excited states with respect to the ground state will not be equal, i.e., $d_i \neq d_j$. Hence, converse to our present model system, the measurement of the CLSs' relative oscillating amplitude and phase can recover how strongly different electronic states or transitions are coupled to the common vibrational modes. It is possible that d_i and d_j may bear different signs, and the resulting CLS oscillations will be π-radians out-of-phase. By studying a general 3LVS using the 2DES, the Huang–Rhys factors for the diagonal peaks and the cross-Huang–Rhys factors for various cross-peaks can be extracted. This procedure will help quantify the relative shifts of the excited state potential minima with respect to the ground state d_i for more complex systems, such as in our earlier study of H_2Pc.[38] In the case of H_2Pc, the electronic states may be coupled to many vibrational modes simultaneously, producing complex beating patterns in the diagonal and cross-peaks, as shown in our earlier study. We note that in our TIPS-Pn study, the intensity of the cross-peak is quite low compared to the diagonal peak (Figs. 5 and S2). However, the noise or the low intensity of the cross-peak, which is due to smaller transition dipole moments or the spectral shape of the interacting pulses, does not, in principle, change the amplitude and the phase of the CLS oscillations. It is, of course, better to have cross-peaks with good intensity for a better estimate of the cross-Huang–Rhys factor. This low intensity increases the noise level to the extracted $\mathrm{CLS}_{ij}(\mathrm{T_w})$ for the cross-peak and complicates the analysis, which results in the measured CLS amplitude having a higher degree of error.

There have been many studies using 2DES to study the oscillations of amplitudes of the peaks.[45–47] The amplitude oscillation arises due to the coupling between the vibrational and the electronic degrees of freedom of the molecule. A coherence created by the pump pulse in the vibrational mode can modulate the electronic state with the period of oscillation of the vibrational mode. The oscillation period of the amplitude of the 2DES peak encodes this periodic modulation of the electronic state by the vibrational mode. Figure 6(a) in our study depicts the oscillations in the integrated intensity of the diagonal and cross-peaks. In Fig. 6(b), we depict the intensity-normalized residual oscillation of the integrated signal for a better comparison of the phases and the amplitudes of the signal oscillations. It is observed in that both the phases and the amplitudes are not similar. Figure S3 of the supplementary material shows the time dependent intensity of various points on the 2DES of the diagonal and cross-peaks. A clear difference in the phase and the amplitude is observed for different points on 2D spectra. Hence, integrating over the peak signal will, in general, give a "random" phase and amplitude depending on the extent of the integration box. In other words, the analysis of the oscillations simply from the peak signal amplitudes, be it single points or integrated over a larger area, may yield no meaningful interpretation of the phase and the amplitude relationships between different peaks. This is to be contrasted with our present analysis using CLS, where there is meaningful information that can be gathered from the definite phases recovered from the oscillations in the CLSs. These phase and amplitude relationships can be traced back to the molecular potential energy surface in terms of shifts of the potential minima of the excited state with respect to the ground state.

We now discuss the non-oscillatory overdamped contributions to the CLS. From Table I, the diagonal peak P_{ii} has one overdamped exponential component with a decay rate constant of ~2.512 ps^{-1} and another, non-decaying overdamped component within our

experimental time window, having an amplitude of 0.088. The ultrafast overdamped component with a rate constant of 2.512 ps^{-1} can be assigned as the inertial solvation arising from the librational motion of the solvent molecules.[27] The second component can be assigned to the diffusive dynamics of the solvent if it decays over several picoseconds[27] or to the structural inhomogeneity of the solute for decay over hundreds of picoseconds to nanoseconds .[28,29] The present set of data concurs with our previous study on TIPS-Pn,[35] where an inertial solvation component was observed with a rate constant in the range ~2.590–3.410 ps^{-1}, which is comparable with our first decay rate constant of ~2.512 ps^{-1} in this study. In our present work, the study of spectral diffusion processes is limited to the delay time window of 2 ps, as we mainly focus on the study of underdamped oscillation of the cross-peak, which lasts about 2 ps. Hence, the non-decaying overdamped component measured here within the experimental time window having an amplitude of 0.088 can be compared with the second component with a mean rate constant of ~0.180 ps^{-1} as measured in our previous study[35] for the diagonal peak. We now discuss the non-oscillatory component of the $CLS_{ij}(T_w)$ of the cross-peak P_{ij}. Within the delay window of 2 ps, it has an almost constant background with negligible exponential decay with an amplitude of ~0.033, which is very small compared to that of the diagonal P_{ii}, which has a non-oscillatory initial $CLS_{ii}(T_w \sim 0)$ of 0.366. This translates to a low effective total covariance[36,38] of $\Lambda_{ij} = 4.8\ ps^{-2}$ compared to the square of the fluctuation amplitude $\Lambda_{ii} = 614\ ps^{-2}$ of the diagonal peak P_{ii}. The total covariance describing the cross-peak can be expressed in the form of frequency fluctuation correlation of two transitions[38] as $\Lambda_{ij} = \langle \delta\omega_i(0)\delta\omega_j(0)\rangle = \langle \delta\omega_i(t)\delta\omega_j(t)\rangle$. It represents the degree of initial correlation between the 0–0 and the 0–1 transition frequencies at the instant when the system converts from the first excited vibrational state to the ground vibrational state for the 1340 cm^{-1} mode. The low covariance Λ_{ij} entails that there is a minimal initial correlation. This can happen when the first excited vibrational state and the ground vibrational state for the 1340 cm^{-1} mode are coupled to different sets of underdamped baths that fluctuate independently. A detailed theoretical study will need to be performed for TIPS-Pn or more complex systems to fully understand the effect on such systems.

CONCLUSION

We theoretically and experimentally studied the delay time dependent peak shape of the 2DES spectra for a model 3LVS, a minimal example of a multi-level system. The molecular system experimentally considered is the spectrally distinct 0–0 and 0–1 vibronic transitions of TIPS-Pn dissolved in toluene, which are separated by 1340 cm^{-1}, corresponding to the short-axis C–C stretching vibration of pentacene. Furthermore, the electronic transition is coupled to a 264 cm^{-1} mode corresponding to the long axis breathing mode of the pentacene moiety in TIPS-Pn. This coupling shows up as oscillations in the CLS measurement in the delay time dependent 2DES spectra. The theoretical model and the resulting simulation corroborate well with the experimentally measured amplitude and the phase of the CLS of the diagonal peak P_{ii}, corresponding to the 0–0 vibronic state, and the cross-peak P_{ij}, corresponding to the combination of "downhill" population transfer from the 0–1 vibronic state to the lower vibronic state 0–0 and the sharing of common ground state by the 0–0 and 0–1 vibronic states. With this proof-of-principle study, using similar approaches of analyzing the CLS of the diagonal and cross-peaks of the 2DES spectra, we estimated quantities such as the cross-Huang Rhys factor, which quantifies how strongly two different transitions are coupled to the common mode. This work complements a related earlier study of the cross-correlated spectral diffusion dynamics of a multi-level system.[38] Furthermore, a more complete picture of the associated FFCF and FXCF of the transitions is recovered, detailing the underdamped and overdamped couplings to the internal molecular modes and external environmental modes. This technique can be a powerful tool to estimate the (cross-) Huang–Rhys factors for various oscillating modes in a complex system by means of the CLS measurement of the 2DES peak, circumventing difficulties of the usual wavelength dependent intensity oscillation across a peak.

SUPPLEMENTARY MATERIAL

The supplementary material contains details on the following: (1) the theoretical calculation of the Huang–Rhys factor for the cross-peak, (2) unscaled 2DES data of TIPS-Pn dissolved in toluene, (3) intensity oscillation of selected points on 2DES of TIPS-Pn, (4) a detailed simulation procedure and the simulated absorption spectra overlaid with the experimental steady-state absorption spectra of TIPS-Pn in toluene, and (5) scaled 2DES spectra for the upper diagonal P_{jj} and the lower cross-peak P_{ji}.

ACKNOWLEDGMENTS

This work was supported by the Singapore Ministry of Education Academic Research Fund (Tier 2 Grant No. MOE-T2EP50122-0022).

AUTHOR DECLARATIONS

Conflict of Interest

The authors have no conflicts to disclose.

Author Contributions

Sanjib Jana: Data curation (equal); Formal analysis (equal); Investigation (equal); Methodology (equal); Software (equal); Visualization (equal); Writing – original draft (equal); Writing – review & editing (equal). **Sachin Prasad**: Methodology (supporting); Visualization (supporting); Writing – review & editing (supporting). **Hoang Long Nguyen**: Investigation (equal); Writing – review & editing (equal). **Duc Viet Le**: Investigation (supporting); Software (equal); Writing – review & editing (supporting). **Howe-Siang Tan**: Conceptualization (equal); Funding acquisition (equal); Investigation (equal); Methodology (equal); Project administration (equal); Resources (equal); Supervision (equal); Writing – review & editing (equal).

DATA AVAILABILITY

The data that support the findings of this study are available from the corresponding author upon reasonable request.

REFERENCES

[1] J. D. Hybl, A. W. Albrecht, S. M. Gallagher Faeder, and D. M. Jonas, "Two-dimensional electronic spectroscopy," Chem. Phys. Lett. **297**(3–4), 307–313 (1998).

[2] D. M. Jonas, "Two-dimensional femtosecond spectroscopy," Annu. Rev. Phys. Chem. **54**(1), 425–463 (2003).

[3] S. Mukamel, "Multidimensional femtosecond correlation spectroscopies of electronic and vibrational excitations," Annu. Rev. Phys. Chem. **51**(1), 691–729 (2000).

[4] F. D. Fuller and J. P. Ogilvie, "Experimental implementations of two-dimensional Fourier transform electronic spectroscopy," Annu. Rev. Phys. Chem. **66**(1), 667–690 (2015).

[5] S. Biswas, J. Kim, X. Zhang, and G. D. Scholes, "Coherent two-dimensional and broadband electronic spectroscopies," Chem. Rev. **122**(3), 4257–4321 (2022).

[6] E. Fresch, F. V. A. Camargo, Q. Shen, C. C. Bellora, T. Pullerits, G. S. Engel, G. Cerullo, and E. Collini, "Two-dimensional electronic spectroscopy," Nat. Rev. Methods Primers **3**(1), 84 (2023).

[7] M. Cho, H. M. Vaswani, T. Brixner, J. Stenger, and G. R. Fleming, "Exciton analysis in 2D electronic spectroscopy," J. Phys. Chem. B **109**, 10542–10556 (2005).

[8] E. L. Read, G. S. Engel, T. R. Calhoun, T. Mančal, T. K. Ahn, R. E. Blankenship, and G. R. Fleming, "Cross-peak-specific two-dimensional electronic spectroscopy," Proc. Natl. Acad. Sci. U. S. A. **104**(36), 14203–14208 (2007).

[9] P. Hamm and M. Zanni, *Concepts and Methods of 2D Infrared Spectroscopy* (Cambridge University Press, 2011).

[10] K. L. M. Lewis and J. P. Ogilvie, "Probing photosynthetic energy and charge transfer with two-dimensional electronic spectroscopy," J. Phys. Chem. Lett. **3**(4), 503–510 (2012).

[11] J. Dostál, J. Pšenčík, and D. Zigmantas, "*In situ* mapping of the energy flow through the entire photosynthetic apparatus," Nat. Chem. **8**(7), 705–710 (2016).

[12] O. Rancova, R. Jankowiak, and D. Abramavicius, "Probing environment fluctuations by two-dimensional electronic spectroscopy of molecular systems at temperatures below 5 K," J. Chem. Phys. **142**(21), 212428 (2015).

[13] V. Butkus, L. Valkunas, and D. Abramavicius, "Molecular vibrations-induced quantum beats in two-dimensional electronic spectroscopy," J. Chem. Phys. **137**(4), 044513 (2012).

[14] V. Butkus, D. Zigmantas, L. Valkunas, and D. Abramavicius, "Vibrational vs. electronic coherences in 2D spectrum of molecular systems," Chem. Phys. Lett. **545**, 40–43 (2012).

[15] J. Seibt and T. Pullerits, "Beating signals in 2D spectroscopy: Electronic or nuclear coherences? Application to a quantum dot model system," J. Phys. Chem. C **117**(36), 18728–18737 (2013).

[16] S. T. Roberts, J. J. Loparo, and A. Tokmakoff, "Characterization of spectral diffusion from two-dimensional line shapes," J. Chem. Phys. **125**(8), 084502 (2006).

[17] S. Bagchi, S. G. Boxer, and M. D. Fayer, "Ribonuclease S dynamics measured using a nitrile label with 2D IR vibrational echo spectroscopy," J. Phys. Chem. B **116**(13), 4034–4042 (2012).

[18] E. Romero, R. Augulis, V. I. Novoderezhkin, M. Ferretti, J. Thieme, D. Zigmantas, and R. Van Grondelle, "Quantum coherence in photosynthesis for efficient solar-energy conversion," Nat. Phys. **10**(9), 676–682 (2014).

[19] J. R. Caram, H. Zheng, P. D. Dahlberg, B. S. Rolczynski, G. B. Griffin, D. S. Dolzhnikov, D. V. Talapin, and G. S. Engel, "Exploring size and state dynamics in CdSe quantum dots using two-dimensional electronic spectroscopy," J. Chem. Phys. **140**(8), 084701 (2014).

[20] K. Kwac and M. Cho, "Two-color pump–probe spectroscopies of two- and three-level systems: 2-dimensional line shapes and solvation dynamics," J. Phys. Chem. A **107**(31), 5903–5912 (2003).

[21] A. Nemeth, F. Milota, T. Mančal, V. Lukeš, J. Hauer, H. F. Kauffmann, and J. Sperling, "Vibrational wave packet induced oscillations in two-dimensional electronic spectra. I. Experiments," J. Chem. Phys. **132**(18), 184514 (2010).

[22] F. Šanda, V. Perlík, C. N. Lincoln, and J. Hauer, "Center line slope analysis in two-dimensional electronic spectroscopy," J. Phys. Chem. A **119**(44), 10893–10909 (2015).

[23] R. Kubo, "A stochastic theory of line shape," Adv. Chem. Phys. **15**, 101–127 (1969).

[24] S. Mukamel, *Principles of Nonlinear Optical Spectroscopy* (Oxford University Press, 1995).

[25] A. Nitzan, *Chemical Dynamics in Condensed Phases: Relaxation, Transfer, and Reactions in Condensed Molecular Systems* (Oxford University Press, 2024).

[26] A. Tokmakoff, "Nonlinear and two-dimensional spectroscopy" (unpublished 2011), available online at https://bpb-us-w2.wpmucdn.com/voices.uchicago.edu/dist/0/1830/files/2019/11/FULL-2D-SPEC-NOTES-2011.pdf (accessed on 10 January 2025).

[27] S. J. Rosenthal, R. Jimenez, G. R. Fleming, P. v. Kumar, and M. Maroncelli, "Solvation dynamics in methanol: Experimental and molecular dynamics simulation studies," J. Mol. Liq. **60**(1–3), 25–56 (1994).

[28] S.-H. Lee, J.-H. Lee, and T. Joo, "Deuterium isotope effect on the solvation dynamics of a dye molecule in methanol and acetonitrile," J. Chem. Phys. **110**(22), 10969–10977 (1999).

[29] S. Park and T. Joo, "Diffractive optics based three-pulse photon echo peak shift studies of spectral diffusion in polar liquids: Evidence for long lived frequency correlations," J. Chem. Phys. **131**(16), 164508 (2009).

[30] K. Kwak, S. Park, I. J. Finkelstein, and M. D. Fayer, "Frequency-frequency correlation functions and apodization in two-dimensional infrared vibrational echo spectroscopy: A new approach," J. Chem. Phys. **127**(12), 124503 (2007).

[31] K. L. Wells, Z. Zhang, J. R. Rouxel, and H.-S. Tan, "Measuring the spectral diffusion of chlorophyll *a* using two-dimensional electronic spectroscopy," J. Phys. Chem. B **117**(8), 2294–2299 (2013).

[32] R. Moca, S. R. Meech, and I. A. Heisler, "Two-dimensional electronic spectroscopy of chlorophyll a: Solvent dependent spectral evolution," J. Phys. Chem. B **119**(27), 8623–8630 (2015).

[33] T. N. Do, M. F. Khyasudeen, P. J. Nowakowski, Z. Zhang, and H. S. Tan, "Measuring ultrafast spectral diffusion and correlation dynamics by two-dimensional electronic spectroscopy," Chem. - Asian J. **14**(22), 3992–4000 (2019).

[34] T. Yoshida and K. Watanabe, "Spectral diffusion of excitons in 3,4,9,10-perylenetetracarboxylic-diimide (PTCDI) thin films," J. Phys. Chem. B **125**(32), 9350–9356 (2021).

[35] D. V. Le, J. M. de la Perrelle, T. N. Do, X. Leng, P. C. Tapping, G. D. Scholes, T. W. Kee, and H.-S. Tan, "Characterization of the ultrafast spectral diffusion and vibronic coherence of TIPS-pentacene using 2D electronic spectroscopy," J. Chem. Phys. **155**(1), 014302 (2021).

[36] M. F. Khyasudeen, P. J. Nowakowski, and H.-S. Tan, "Measuring the ultrafast correlation dynamics between the Q_x and Q_y bands in chlorophyll molecules," J. Phys. Chem. B **123**(6), 1359–1364 (2019).

[37] J. Sung and R. J. Silbey, "Optical four wave mixing spectroscopy for multilevel systems coupled to multimode Brownian oscillators," J. Chem. Phys. **118**(5), 2443–2445 (2003).

[38] S. Jana, T. N. Do, P. J. Nowakowski, M. F. Khyasudeen, D. V. Le, I. J. Y. Lim, S. Prasad, J. Zhang, and H.-S. Tan, "Measuring the ultrafast correlation dynamics of a multilevel system using the center line slope analysis in two-dimensional electronic spectroscopy," J. Phys. Chem. B **127**(33), 7309–7322 (2023).

[39] M. Khalil, N. Demirdöven, and A. Tokmakoff, "Coherent 2D IR spectroscopy: Molecular structure and dynamics in solution," J. Phys. Chem. A **107**(27), 5258–5279 (2003).

[40] J. Sung and R. J. Silbey, "Four wave mixing spectroscopy for a multilevel system," J. Chem. Phys. **115**(20), 9266–9287 (2001).

[41] M. Cho, "Coherent two-dimensional optical spectroscopy," Chem. Rev. **108**(4), 1331–1418 (2008).

[42] D. T. James, B. K. C. Kjellander, W. T. T. Smaal, G. H. Gelinck, C. Combe, I. McCulloch, R. Wilson, J. H. Burroughes, D. D. C. Bradley, and J.-S. Kim, "Thin-film morphology of inkjet-printed single-droplet organic transistors using polarized Raman spectroscopy: Effect of blending TIPS-pentacene with insulating polymer," ACS Nano **5**(12), 9824–9835 (2011).

[43] M. Cho, *Two-Dimensional Optical Spectroscopy* (CRC Press, 2009).

[44] Z. Zhang, K. L. Wells, E. W. J. Hyland, and H.-S. Tan, "Phase-cycling schemes for pump–probe beam geometry two-dimensional electronic spectroscopy," Chem. Phys. Lett. **550**, 156–161 (2012).

[45]A. A. Bakulin, S. E. Morgan, T. B. Kehoe, M. W. B. Wilson, A. W. Chin, D. Zigmantas, D. Egorova, and A. Rao, "Real-time observation of multiexcitonic states in ultrafast singlet fission using coherent 2D electronic spectroscopy," Nat. Chem. **8**(1), 16–23 (2016).
[46]J. D. Schultz, T. Kim, J. P. O'Connor, R. M. Young, and M. R. Wasielewski, "Coupling between harmonic vibrations influences quantum beating signatures in two-dimensional electronic spectra," J. Phys. Chem. C **126**(1), 120–131 (2022).
[47]J.-Y.-R. Jin, H.-Y. Zhang, Y.-X. Yao, R.-H. Chen, and Q. Ai, "Observing quantum coherent oscillations in a three-level atom via electromagnetically induced transparency by two-dimensional spectroscopy," J. Chem. Phys. **162**(1), 014112 (2025).